Smart Structures and Systems, *Vol. 29, No. 6 (2022) 767-775*
https://doi.org/10.12989/sss.2022.29.6.767

In situ monitoring-based feature extraction for metal additive manufacturing products warpage prediction

Jungeon Lee[1a], Adrian M. Chung Baek[2b], Namhun Kim[2c] and Daeil Kwon*[1]

[1]*Department of Industrial Engineering, Sungkyunkwan University, 2066, Seobu-ro, Jangan-gu, Suwon 16419, Republic of Korea*
[2]*Department of Mechanical Engineering, Ulsan National Institute of Science and Technology, 50, UNIST-gil, Eonyang-eup, Ulsan 44919, Republic of Korea*

(*Received October 31, 2021, Revised March 20, 2022, Accepted April 25, 2022*)

Abstract. Metal additive manufacturing (AM), also known as metal three-dimensional (3D) printing, produces 3D metal products by repeatedly adding and solidifying metal materials layer by layer. During the metal AM process, products experience repeated local melting and cooling using a laser or electron beam, resulting in product defects, such as warpage, cracks, and internal pores. Such defects adversely affect the final product. This paper proposes the in situ monitoring-based warpage prediction of metal AM products with experimental feature extraction. The temperature profile of the metal AM substrate during the process was experimentally collected. Time-domain features were extracted from the temperature profile, and their relationships to the warpage mechanism were investigated. The standard deviation showed a significant linear correlation with warpage. The findings from this study are expected to contribute to optimizing process parameters for metal AM warpage reduction.

Keywords: experimental validation; feature extraction; *in situ* monitoring; metal additive manufacturing; warpage prediction

1. Introduction

Metal additive manufacturing (AM) is used to manufacture metal products with complex shapes or to repair damaged metal parts. Metal AM can achieve the desired shape with less preparation and waste than other metal manufacturing processes, such as casting, forming, and cutting. Owing to this advantage, metal AM has been widely applied in industrial fields, such as aerospace, automotive, and machining industries (Lee *et al*. 2018, Kumar and Nair 2017, Vafadar *et al*. 2021). AM process repeatedly adds and joins materials typically using melting and solidifying cycles to build the final product. For the metal AM process, a laser or electron beam is used for joining, referred to as a deposition. During deposition, metal AM products often undergo nonlinear and transient thermal conditions that can cause thermal deformations (Frazier 2014, Matsunawa *et al*. 2003, Zeng *et al*. 2016, Lewandowski and Seifi 2016, Stavropoulos and Foteinopoulos 2018).

Studies have been conducted to predict and reduce thermal deformation. A common strategy is to adjust the process parameters and identify their effects on thermal deformation. Several studies have noted that different process parameter settings significantly affect thermal conditions and deformations (Foroozmehr and Kovacevic 2010, Rubino *et al*. 2018, Shi *et al*. 2006, Srivastava *et al*. 2021). The process parameters are the input variables such as scan path, scan speed, and laser power. The process parameters are predetermined before the process starts according to the materials used, product design, or desired processing time. Paul *et al*. (2014) applied numerical simulations to identify the effects of process parameters on thermal deformation in the metal AM process, finding that layer thickness and part orientation were correlated with the occurrence of thermal deformation. Foroozmehr and Kovacevic (2010) found that the thermal deformation of the substrate was reduced more when a zigzag scan path was applied than when a spiral scan path was applied. Through numerical simulation, the authors also found that the sample printed with the spiral scan path exhibited a less uniform temperature distribution than the others. Rubino *et al*. (2018) suggested that lowering the scan speed may decrease the thermal deformation of the final product. Additionally, the thermal load that induced thermal stresses and deformation was numerically calculated.

Another strategy is to apply *in situ* monitoring (Khanzadeh *et al*. 2018, Lee and Chung 2020, Arnold and Körner 2021). Through *in situ* monitoring, process, product temperature, and thermal image data can be measured to predict the thermal deformation of a product as they are direct indicators of the thermal conditions. One additional advantage of an *in situ* monitoring-based strategy is that several uncertainties that may intervene during the actual process can also be considered. For example, in addition to the process parameter settings, poor equipment conditions and material quality can also change the thermal conditions and cause thermal deformation. Arnold and Körner (2021) suggested that electron-optical images of the product during

*Corresponding author, Professor
E-mail: dikwon@skku.edu

ISSN: 1738-1584 (Print), 1738-1991 (Online)

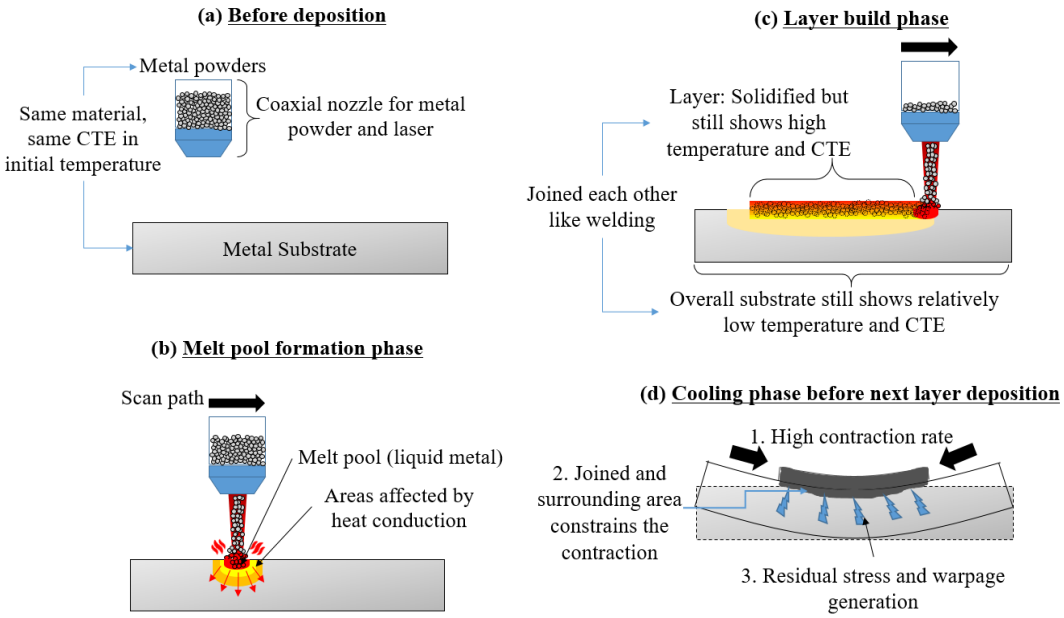

Fig. 1 Schematic of the DED process and following warpage mechanism

the process could be used as *in situ* monitoring methods for predicting thermal deformations. Image features are extracted to quantify the amount of thermal deformation generated in each layer, and the total deformation is predicted. By using *in situ* temperature monitoring, Lee and Chung (2020) suggested that the temperature profile of the product during the process can be used to identify its thermal conditions. Further, different temperature profiles resulted in different thermal-deformation modes. The key activity of an *in situ* monitoring-based strategy is determining which measurements and features can be used to identify and quantify the thermal conditions.

In this study, an *in situ* monitoring-based feature extraction method for metal AM product defect prediction is proposed. This study focuses on the thermal deformation (i.e., warpage) of the substrate. Metal AM products are deposited on a base metal plate (i.e., substrate). When thermal deformation occurs in the substrate, all subsequent layers and final products are ultimately deformed (Li *et al*. 2018, Caltanissetta *et al*. 2018). The thermal conditions during the process are measured using an *in situ* temperature profile, and the time-domain features are extracted for quantification. Section 2 introduces our research background and approach. Section 3 presents the experimental procedures for *in situ* temperature monitoring and warpage measurements. Section 4 presents the results and a discussion of the proposed method. Section 5 summarizes the study and provides conclusions and recommendations for future research.

2. Background

This section introduces the warpage mechanism in the metal AM process and feature engineering methods, including time-domain feature extraction and selection methods.

2.1 Warpage mechanism in metal AM process

This study focuses on the direct energy deposition (DED) metal AM process. Fig. 1 shows a schematic of the DED process. First, a 3D digital model of the product is introduced into the DED software and sliced into nearly two-dimensional (2D) layers with a thickness of a few micrometers or millimeters. A powder nozzle with a laser source moves through the scan path, melting a small area of the substrate to create a melt pool (Fig. 1(b)). Simultaneously, metal powders are supplied to deposit the 2D shape of the layer (Fig. 1(c)). When the deposition for one layer is completed, the next layer is deposited and repeated to fabricate a 3D shape (Fig. 1(a)-(c) are repeated).

During deposition, metal AM products often undergo nonlinear and transient thermal conditions, which can cause warpage. The metal AM substrate warpage mechanism can be explained by differences in the coefficient of thermal expansion (CTE) within the body caused by the nonlinear and transient thermal conditions (Li *et al*. 2018, Paul *et al*. 2014). CTE is a material property that indicates the expansion and contraction rates based on temperature changes (Gere and Goodno 2009). A material with a higher CTE expands and contracts more than others under the same temperature change. It has been experimentally reported that the CTE of most metal materials used in metal AM is a temperature-dependent variable, as shown in Fig. 2 (Desai and Ho 1978). Fig. 1 presents a schematic of the warpage mechanism during DED process. Because the laser beam locally irradiates the top of the substrate during the process, as can be seen in Fig. 1(b), the printed layer shows a higher CTE than the substrate, as can be seen in Fig. 1(c). In the layer-build phase, the solidified layer is in a thermally expanded state. As the layer and the substrate are joined, it can be considered as one solid body; however, it has a locally uneven temperature and CTE distribution. During the cooling phase, the layer with a high CTE shrinks

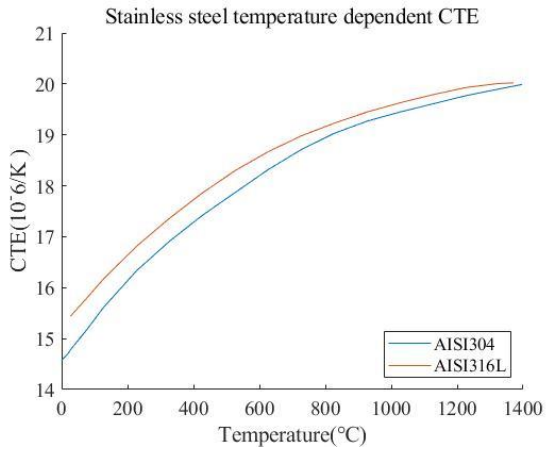

Fig. 2 Temperature-dependent CTE of AISI 316L and AISI 304 stainless steel

more, while the surrounding substrate and joined area with a relatively low CTE constrain them, generating residual stresses (Fig. 1(d)). This stress accumulates as the layer stacks and eventually leads to warpage if it exceeds the yield strength of the substrate (Venkatkumar *et al*. 2016).

2.2 Time-domain feature extraction

In this study, time-domain features were extracted from the substrate temperature profile and analyzed for warpage prediction. Time-domain features are statistical values that can be extracted from data collected against time, such as vibration, noise, or temperature (Sim *et al*. 2020). Extracted features can show the condition of system, such as defect occurrences or degradation. Time-domain feature extraction is widely applied in industrial systems, such as rotating machinery, motor, or engine, for the defect diagnosis and prediction (Sim *et al*. 2020, Wang *et al*. 2019, Kim*et al*. 2020). Table 1 lists the general time-domain features which can be extracted from the data. Several features do not have physical meanings related to the system, but they show experimentally good performances. Others have physical meaning that can be explained by domain knowledge. For example, the peak value of the vibration signal of a rotating machinery represents the magnitude of the vibration. Conversely, the root mean square (RMS) values are not related to any physical meaning. However, both features generally increase as the degree of the fault increases.

2.3 Statistical feature selection

After feature extraction, statistical feature selection can be applied to identify features that are significantly correlated with warpage. Pearson correlation analysis is a generally applicable feature selection method for regression problem. The Pearson correlation coefficient (r) quantifies the linear correlation between two variables, X and Y. In this study, each variable represents the time-domain feature and warpage, respectively. A Pearson correlation coefficient with a value between -1 and +1. r=+1 represents a perfect positive linear correlation, r=0 represents no linear correlation, and r=-1 represents a perfect negative linear

Table 1 General time-domain features

Feature	Formula	Statistical meaning
Mean	$\frac{\sum X}{N}$	Average value of data
Peak	$\mathrm{Max}(\lvert X\rvert)$	Maximum value of data
Peak to peak (p2p)	$\mathrm{Max}(X)$ - $\mathrm{Min}(X)$	Difference between maximum and minimum value
Root mean square (RMS)	$\sqrt{\frac{\sum X^2}{N}}$	Square root of the mean square
Standard deviation (STD)	$\sqrt{\frac{\sum(X-\bar{X})^2}{N-1}}$	Value representing the dispersion of data
Skewness	$\frac{\frac{1}{N}\sum(X-\bar{X})^3}{STD^3}$	Asymmetry of the probability distribution
Kurtosis	$\frac{\frac{1}{N}\sum(X-\bar{X})^4}{STD^4}$	Sharpness of the probability distribution
Crest factor (CF)	$\frac{Peak}{RMS}$	Peak considering RMS value
Impulse factor (IF)	$\frac{Peak}{absMean}$	Peak considering absolute value
Shape factor (SF)	$\frac{RMS}{absMean}$	Degree of graph variation

correlation. Through Pearson correlation analysis, features having a high correlation with warpage can be identified and used for more accurate warpage prediction. The prediction performance of the feature is evaluated by the coefficient of determination. The coefficient of determination (r^2, R^2) represents the proportion of variation in the dependent variable, Y, which is predictable from the independent variable, X. The coefficient of determination has a value between zero and one.

3. Experimental procedures

This section introduces the experimental setup, including the process parameter settings, sample design, and data acquisition methods.

3.1 Process parameters and sample design

Experiments were conducted using an Insstek® MX-600 DED metal AM machine. AISI316L stainless steel powder and AISI304 stainless steel were selected as the deposition material and substrate material, respectively. Substrate and powder with similar material are commonly selected to reduce warpage caused by differences in material CTEs.

Table 2 lists the fixed process parameters that were experimentally validated as optimal for depositing stainless steel. The scan-path width was set to 0.8 mm according to the beam diameter; however, it was reported that the scan-path width is laser power dependent variable (Choi 2020).

In this study, two process parameters, laser power and scan path, were selected as variables based on previous studies (Foroozmehr and Kovacevic 2010, Lee and Chung 2020, Bian *et al*. 2020). Fig. 3 shows three different scan-path parameter settings. The selected parameters were adjusted for each experiment to reproduce various substrate temperature profile. A total of 45 substrate temperature-

Table 2 Fixed process parameters

Process Parameters	Value
Powder feeding rate (g/min)	3.50±0.1
Coaxial gas rate (L/min)	4.0
Carrier gas rate (L/min)	2.5
Coaxial/Carrier gas composition	Argon, purity 99.999%
Beam diameter (mm)	0.8
Nozzle distance (mm)	9
Layer thickness (mm)	0.25
Nozzle speed (m/min)	0.85
Substrate material	SUS304
Substrate size (mm)	75×100×10 (WDH)
Powder material	SUS316L
Powder size (μm)	45 to 150
Hatch space (mm)	0.4

Table 3 Different process parameter settings

Tool path \ Laser power	250 W	300 W	350 W	400 W	450 W
Transverse	3	3	3	3	3
Longitudinal	3	3	3	3	3
Spiral in	3	3	3	3	3

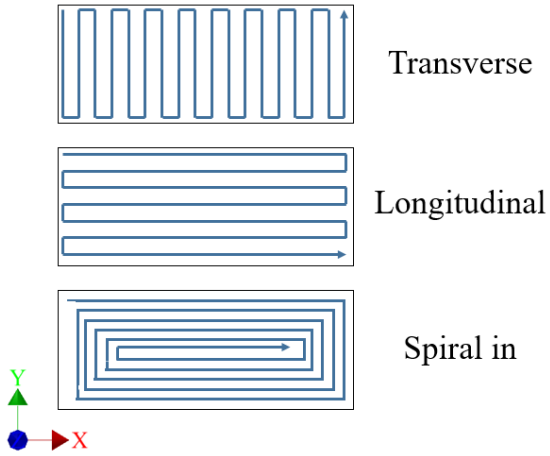

Fig. 3 Schematic of three difference scan paths

warpage datasets were collected, as listed in Table 3. Experiments were conducted using 15 different process parameter settings, and each experiment was repeated three times to ensure repeatability.

Fig. 4 shows a schematic of the sample description. The dimensions of the substrate were 100×75×10 mm, and those of the printed part were 75×30×5 mm. To exclude the effect of additional distortion caused by the rearrangement of the residual stress, the warpage of the substrate was measured without removing the part from the substrate.

3.2 In situ temperature monitoring

For *in situ* temperature monitoring, a high-temperature glass-fiber insulated (up to 480°C) K-type thermocouple with a diameter of 0.127 mm was selected. The thermocouples were attached to the backside of the

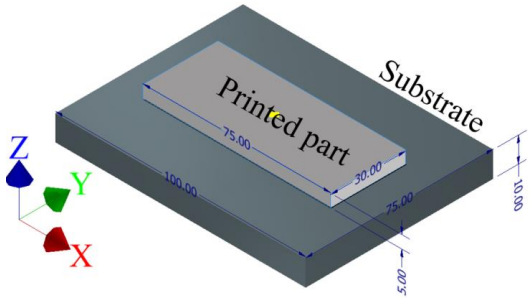

Fig. 4 Schematic of sample description (mm)

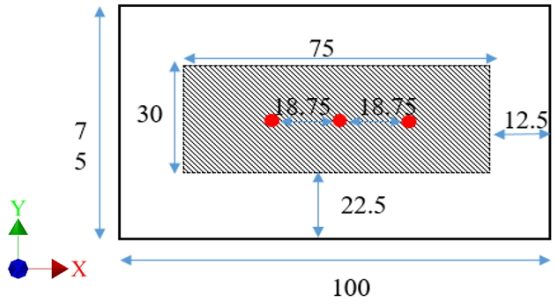

Fig. 5 Schematic of printing sample with thermocouple attached locations (mm)

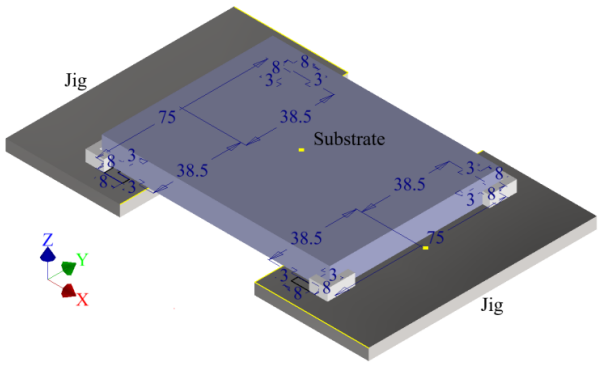

Fig. 6 Schematic of jigs and substrate (mm)

substrate to avoid measurement errors and noise caused by excessively high temperatures (Zhang *et al.* 2021). The temperature profile of the substrate was collected as a time series using an Agilent 34970A module at a sampling rate of 1 Hz.

Two jigs were used to lift and fix the substrate 5 mm from the bed to attach the thermocouple to the backside. The jig constrained the *x*- and *y*-directions of the substrate, as shown in Fig. 6 and Fig. 7. Owing to the friction between the jig wall and the substrate, the substrate was partially constrained in the z-direction. Such constraints can result in less warpage. Nonetheless, considerable warpage was observed.

3.3 Warpage data acquisition

In this study, the quantitative value of the warpage of the substrate is defined as the maximum distance between the warpage curve and reference plane. The warpage of the substrate was measured in a one-dimensional (1D) linear form using a Mitutoyo® SV-C3100 form-tracer. The

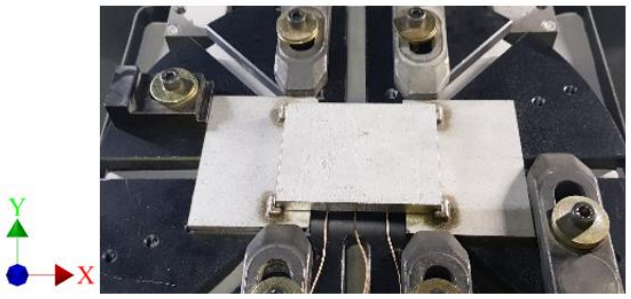

Fig. 7 Substrate constrained in the *x*- and *y*-directions with the jigs

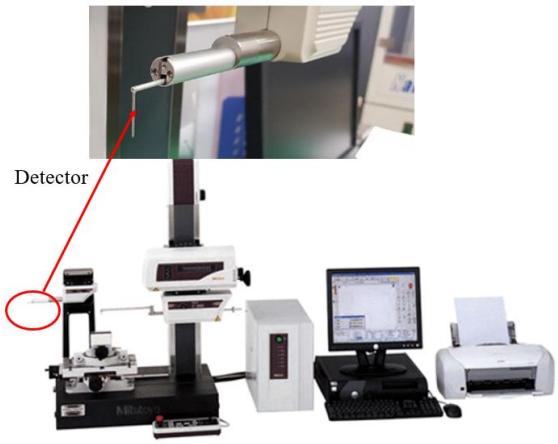

Fig. 8 Mitutoyo® SV-C3100 form-tracer

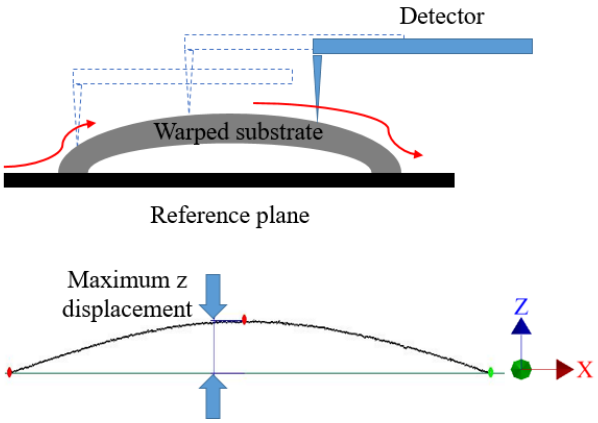

Fig. 9 Schematic of warpage measurement process

surface profile curve of the substrate was measured via contact with the detector, as shown in Fig. 8. The speed of the detector and the sampling rate were 1 mm/s and 50 Hz, respectively.

After measuring the linear curvature of the substrate, the reference plane was determined to identify the maximum height between the plane and curvature. Fig. 9 shows a schematic of the warpage measurement process with the actual measured warpage profile. Because the form-tracer can only measure 1D linear warpage, it may not sufficiently reflect the warpage of the surface. To estimate the overall warpage of the substrate, each substrate was measured with six different lines, as shown in Fig. 10, and the mean value was selected (Dastjerdi *et al*. 2017).

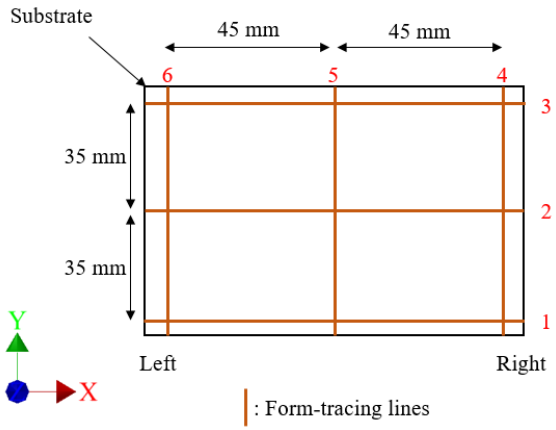

Fig. 10 Form-tracing method to estimate surface warpage

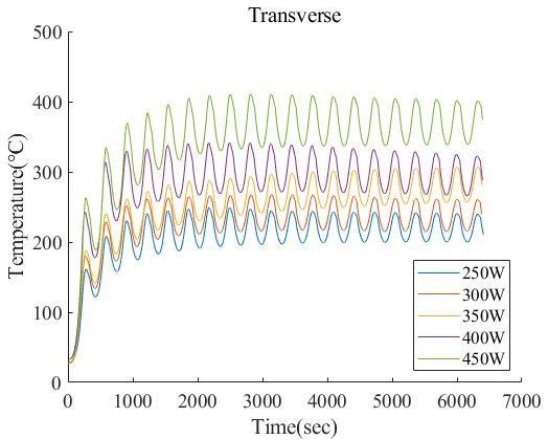

Fig. 11 Difference in temperature profile according to laser power (transverse scan path)

4. Experimental results and discussion

This section presents the experimental results and analysis. Time-series features were extracted from the substrate temperature, and their correlation with warpage was presented. Some features that exhibit a better performance are explained based on the warpage mechanism.

4.1 Temperature profile analysis

Fig. 11-13 show the differences in temperature profile according to laser power setting. For all scan-path settings, as the laser power increased, the overall temperature of the substrate increased. Fig. 14 and Fig. 15 show the differences in temperature profile according to the scan path. Significant difference in the shape of the temperature profile was found, depending on the scan-path setting. Time-domain features were extracted to quantitatively identify such difference in temperature profile according to the process parameter settings, and for warpage prediction.

4.2 Time-domain feature extraction and selection for warpage prediction

Table 4 shows the correlation and determination

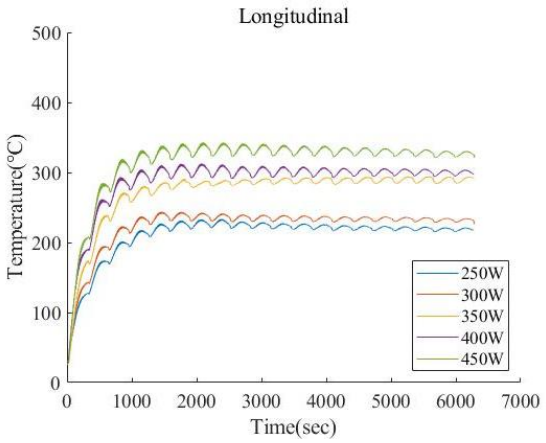

Fig. 12 Difference in temperature profile according to laser power (longitudinal scan path)

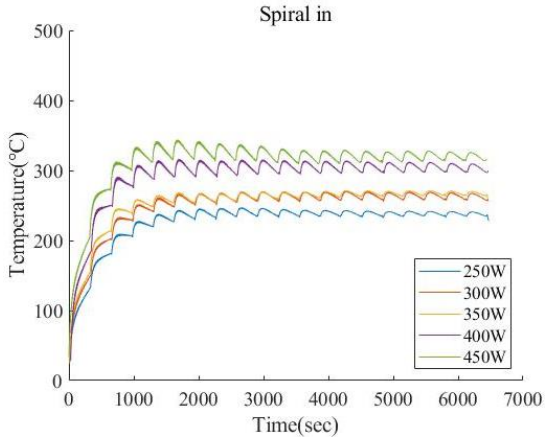

Fig. 13 Difference in temperature profile according to laser power (spiral in scan path)

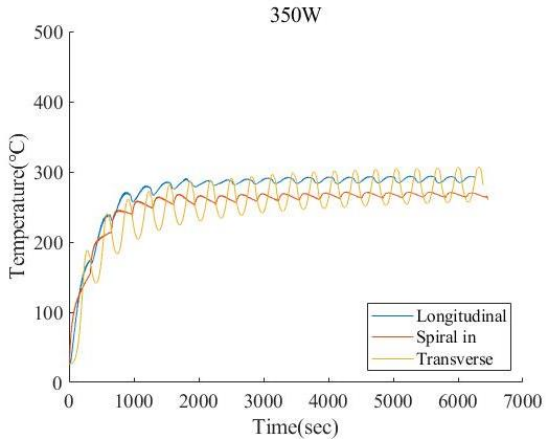

Fig. 14 Difference in temperature profile according to scan path (nominal laser power 350 W)

coefficients between each feature and warpage. Fig. 16 and Fig. 17 show bar plots for warpage prediction performance comparison of the features. Fig. 18-23 show scatterplots of STD, mean, RMS, and kurtosis between warpages.

The standard deviation (STD) showed the most significant performance in terms of the linear correlation with warpage. It can be seen that the scatter plot of STD

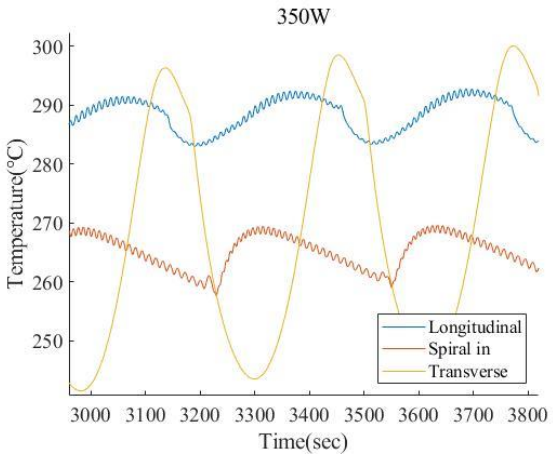

Fig. 15 Enlarged graph of difference in temperature profile according to scan path

Table 4 Correlation and determination coefficients between each feature and warpage

Feature	Correlation coefficient (*r*)	Coefficient of determination (*r* squared)
Mean	0.536	0.287
Peak	0.765	0.585
Peak to peak (p2p)	0.767	0.588
Root mean square (RMS)	0.558	0.312
Standard deviation (STD)	0.892	0.796
Skewness	0.652	0.425
Kurtosis	0.55	0.302
Crest factor (CF)	0.786	0.618
Impulse factor (IF)	0.789	0.623
Shape factor (SF)	0.756	0.571

and warpage is tightly distributed along the regression line. This result can relate to the warpage mechanism. The STD can represent the non-uniformity of the temperature profile because it statistically refers to the deviation of the temperature change during the process. A large STD indicates that the product has undergone significant temperature changes during the process, resulting large CTE differences. Several numerical studies have shown that non-uniform temperatures can cause large warpages. Foroozmehr and Kovacevic (2010) reported that a DED sample printed with a spiral scan path showed a non-uniform temperature distribution during the process, resulting in the largest residual stress. However, because the analysis was performed as a numerical simulation, the non-uniformity of temperature was not quantitatively defined, as was the experimental feature introduced in the current study. Bian *et al*. (2020) reported that the residual stress was larger under a striped scanning path and a higher laser power. The numerical simulation results indicated that the stripe scan path generated a higher temperature gradient for the product during the process. Additionally, warpage caused by non-uniform temperature is a common phenomenon found in other metal processes, such as injection molding, casting, and sheet-forming (Sánchez *et*

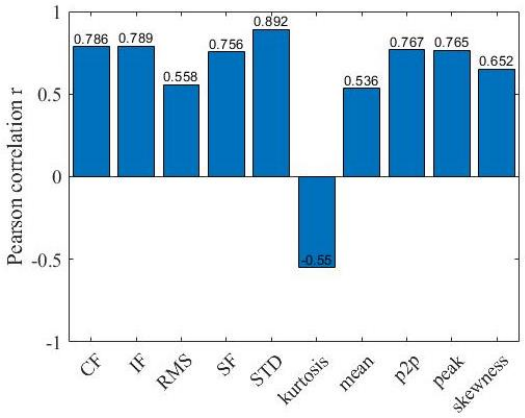

Fig. 16 Pearson correlation coefficient (*r*) comparison between each feature and warpage

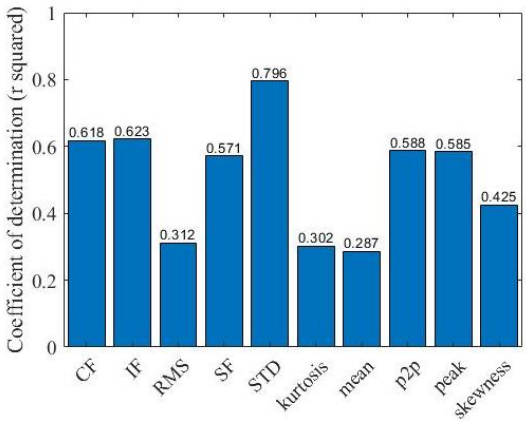

Fig. 17 Coefficient of determination (R^2) comparison between each feature and warpage

al. 2012, Mageshwaran *et al*. 2017, Kyrsanidi *et al*. 2000).

The mean, RMS, and kurtosis showed significantly lower performances than the others. The mean and RMS of temperature may be related to the changes in material properties, especially CTE changes, during the process. Based on the warpage mechanism, higher temperatures result in a larger CTE difference and lower yield stress in the material; thus, warpage can easily occur. Bian *et al*. (2020) noted that when a high laser power is applied, significant residual stress is generated as the melt pool becomes larger and undergoes higher temperatures. However, the experimental results of the study in question contrasted the theoretical background. For the mean temperature, the repeated movement of the nozzle may have led to a loss of meaning. Fig. 11-15 show examples of time-series temperature data collected during the process. Owing to the nature of the DED process, in which the nozzle moves repeatedly along a predetermined scan path, the temperature profile shows a repeated waveform. With this type of data, the mean may lose its meaning as a representative value. Additionally, because the process does not show any negative temperature, the RMS can also lose its meaning, like the mean value. Generally, the peak or p2p values are considered more robust than the mean or RMS for such repetitive waveforms (Sim *et al*. 2020). The current results confirm that the performances of the peak and p2p

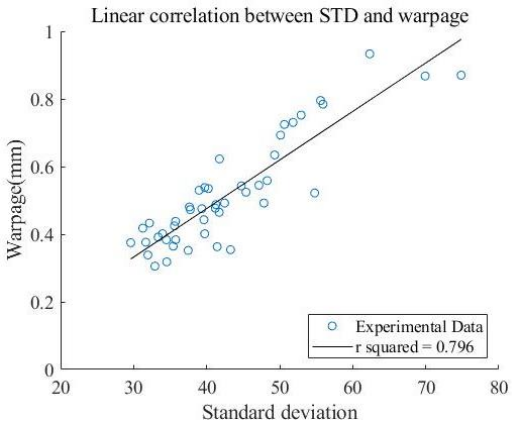

Fig. 18 Scatterplot of STD and warpage

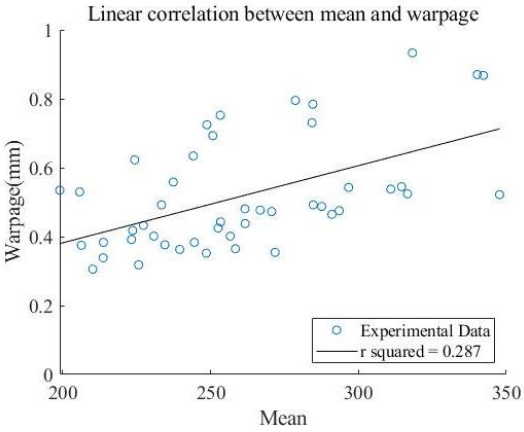

Fig. 19 Scatterplot of mean and warpage

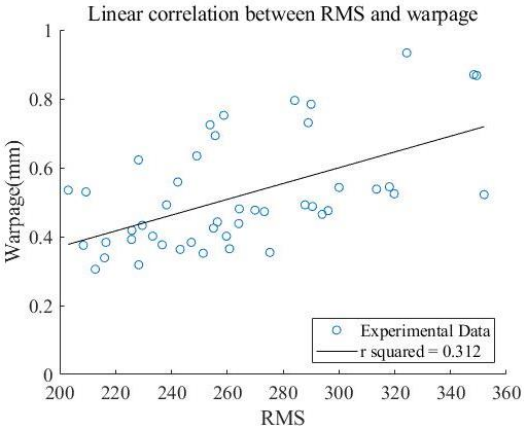

Fig. 20 Scatterplot of RMS and warpage

were better than those of the mean and RMS. Both the feature and original data should be considered when analyzing temperature data in the metal AM process. The physical meaning of the remaining features, including kurtosis, has not yet been defined and remains a future challenge.

5. Conclusions

This study suggested an *in situ* monitoring-based feature

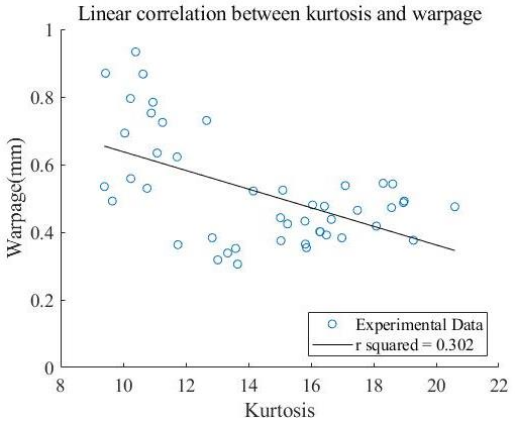

Fig. 21 Scatterplot of kurtosis and warpage

extraction method for metal AM defect prediction with experimental validation. The temperature profile of the substrate was collected, and time-domain features were extracted. To identify the significant features for warpage prediction, the correlation between each feature and warpage was identified. Furthermore, the physical meanings of the features, which can be explained by the warpage mechanism, were identified. The STD showed a significant linear correlation with warpage. Based on current research, the authors plan to develop a more accurate warpage prediction method in the near future.

The authors expect that the proposed method will contribute to warpage reduction in metal AM products. Furthermore, the proposed methodology is expected to apply to other manufacturing processes with similar defect occurrence mechanisms, such as injection molding, casting, and sheet-forming.

Acknowledgments

This research was supported by a National Research Foundation of Korea (NRF) grant funded by the Korean government (MSIT) (NRF-2020R1A4A407990411) and a Korea Institute for Advancement of Technology (KIAT) grant funded by the Korean government (MOTIE) (N0002429, The Competency Development Program for Industry Specialist).

References

Arnold, C. and Körner, C. (2021), "In-situ electron optical measurement of thermal expansion in electron beam powder bed fusion", *Add. Manuf.*, **46**, 102213. https://doi.org/10.1016/j.addma.2021.102213.

Bian, P., Shi, J., Liu, Y. and Xie, Y. (2020), "Influence of laser power and scanning strategy on residual stress distribution in additively manufactured 316L steel", *Optic. Las. Technol.*, **132**, 106477. https://doi.org/10.1016/j.optlastec.2020.106477.

Caltanissetta, F., Grasso, M., Petro, S. and Colosimo, B.M. (2018), "Characterization of in-situ measurements based on layerwise imaging in laser powder bed fusion", *Add. Manuf.*, **24**, 183-199. https://doi.org/10.1016/j.addma.2018.09.017.

Choi, T.Y. (2020), "Machine learning based predictive modeling of dimensional quality in direct energy deposition with SUS316L", Graduate School of UNIST.

Dastjerdi, A.A., Movahhedy, M.R. and Akbari, J. (2017), "Optimization of process parameters for reducing warpage in selected laser sintering of polymer parts", *Add. Manuf.*, **18**, 285-294. https://doi.org/10.1016/j.addma.2017.10.018.

Desai, P.D. and Ho, C.Y. (1978), "Thermal linear expansion of nine selected AISI stainless steels", Thermophysical and Electronic Properties Information Analysis Center Lafayette In.

Foroozmehr, E. and Kovacevic, R. (2010), "Effect of path planning on the laser powder deposition process: Thermal and structural evaluation", *Int. J. Adv. Manuf. Technol.*, **51**(5), 659-669. https://doi.org/10.1007/s00170-010-2659-6.

Frazier, W.E. (2014), "Metal additive manufacturing: A review", *J. Mater. Eng. Perform.*, **23**(6), 1917-1928. https://doi.org/10.1007/s11665-014-0958-z.

Gere, J.M. and Goodno, B.J. (2009), *Mechanics of Materials*, Cengage Learning. Inc., Independence, KY.

Khanzadeh, M., Chowdhury, S., Marufuzzaman, M., Tschopp, M.A. and Bian, L. (2018), "Porosity prediction: Supervised-learning of thermal history for direct laser deposition", *J. Manuf. Syst.*, **47**, 69-82. https://doi.org/10.1016/j.jmsy.2018.04.001.

Kim, Y.W. and Jewong, W.B. (2020), "Defect classification of refrigerant compressor using variance estimation of the transfer function between pressure pulsation and shell acceleration", *Smart Struct. Syst.*, **25**(2), 255-264. https://doi.org/10.12989/sss.2020.25.2.255.

Kumar, L.J. and Krishnadas Nair, C.G. (2017), "Current trends of additive manufacturing in the aerospace industry", *Advances in 3D Printing & Additive Manufacturing Technologies*, Springer, Singapore.

Kyrsanidi, A.K., Kermanidis, T.B. and Pantelakis, S.G. (2000), "An analytical model for the prediction of distortions caused by the laser forming process", *J. Mater. Proc. Technol.*, **104**(1-2), 94-102. https://doi.org/10.1016/S0924-0136(00)00520-3.

Lee, J. and Chung, H. (2020), "Experimental investigation of deposition pattern on the temperature and distortion of direct energy deposition-based additive manufactured part", *Appl. Sci.*, **10**(21), 7653. https://doi.org/10.3390/app10217653.

Lee, Y., Lee, S., Zhao, X.G., Lee, D., Kim, T., Jung, H. and Kim, N. (2018), "Impact of UV curing process on mechanical properties and dimensional accuracies of digital light processing 3D printed objects", *Smart Struct. Syst.*, **22**(2), 161-166. https://doi.org/10.12989/sss.2018.22.2.161.

Lewandowski, J.J. and Seifi, M. (2016), "Metal additive manufacturing: A review of mechanical properties", *Ann. Rev. Mater. Res.*, **46**, 151-186. https://doi.org/10.1146/annurev-matsci-070115-032024.

Li, C., Liu, Z.Y., Fang, X.Y. and Guo, Y.B. (2018), "Residual stress in metal additive manufacturing", *Procedia Cirp*, **71**, 348-353. https://doi.org/10.1016/j.procir.2018.05.039.

Mageshwaran, G., Polisetti, S.R., Jeevahan, J. and Joseph, G.B. (2017), "Enhancement of uniform temperature distribution during casting solidification by methoding process", *Int. J. Ambient Energy*, **38**(8), 774-780. https://doi.org/10.1080/01430750.2016.1222959.

Matsunawa, A., Mizutani, M., Katayama, S. and Seto, N. (2003), "Porosity formation mechanism and its prevention in laser welding", *Weld. Int.*, **17**(6), 431-437. https://doi.org/10.1533/wint.2003.3138.

Paul, R., Anand, S. and Gerner, F. (2014), "Effect of thermal deformation on part errors in metal powder based additive manufacturing processes", *J. Manuf. Sci. Eng.*, **136**(3), 031009. https://doi.org/10.1115/1.4026524.

Rubino, F., Astarita, A. and Carlone, P. (2018), "Thermo-mechanical finite element modeling of the laser treatment of titanium cold-sprayed coatings", *Coating.*, **8**(6), 219.

https://doi.org/10.3390/coatings8060219.

Sánchez, R., Aisa, J., Martinez, A. and Mercado, D. (2012), "On the relationship between cooling setup and warpage in injection molding", *Measure.*, **45**(5), 1051-1056. https://doi.org/10.1016/j.measurement.2012.01.039.

Shi, Y., Yao, Z., Shen, H. and Hu, J. (2006), "Research on the mechanisms of laser forming for the metal plate", *Int. J. Mach. Tool. Manuf.*, **46**(12-13), 1689-1697. https://doi.org/10.1016/j.ijmachtools.2005.09.016.

Sim, J., Kim, S., Park, H.J. and Choi, J.H. (2020), "A tutorial for feature engineering in the prognostics and health management of gears and bearings", *Appl. Sci.*, **10**(16), 5639. https://doi.org/10.3390/app10165639.

Srivastava, S., Garg, R.K., Sharma, V.S. and Sachdeva, A. (2021), "Measurement and mitigation of residual stress in wire-arc additive manufacturing: A review of macro-scale continuum modelling approach", *Arch. Comput. Meth. Eng.*, **28**(5), 3491-3515. https://doi.org/10.1007/s11831-020-09511-4.

Stavropoulos, P. and Foteinopoulos, P. (2018), "Modelling of additive manufacturing processes: A review and classification", *Manuf. Rev.*, **5**, 2. https://doi.org/10.1051/mfreview/2017014.

Vafadar, A., Guzzomi, F., Rassau, A. and Hayward, K. (2021), "Advances in metal additive manufacturing: A review of common processes, industrial applications, and current challenges", *Appl. Sci.*, **11**(3), 1213. https://doi.org/10.3390/app11031213.

Venkatkumar, D. and Ravindran, D. (2016), "3D finite element simulation of temperature distribution, residual stress and distortion on 304 stainless steel plates using GTA welding", *J. Mech. Sci. Technol.*, **30**(1), 67-76. https://doi.org/10.1007/s12206-015-1208-5.

Wang, H., Zhu, Q., Li, J., Mao, J., Hu, S. and Zhao, X. (2019), "Identification of moving train loads on railway bridge based on strain monitoring", *Smart Struct. Syst.*, **23**(3), 263-278. https://doi.org/10.12989/sss.2019.23.3.263.

Zeng, C., Tian, W., Liao, W.H. and Hua, L. (2016), "Microstructure and porosity evaluation in laser-cladding deposited Ni-based coatings", *Surf. Coating. Technol.*, **294**, 122-130. https://doi.org/10.1016/j.surfcoat.2016.03.083.

Zhang, Z., Liu, Z. and Wu, D. (2021), "Prediction of melt pool temperature in directed energy deposition using machine learning", *Add. Manuf.*, **37**, 101692. https://doi.org/10.1016/j.addma.2020.101692.